

Understanding the Dynamics Governing Electrocatalytic Hydrodeoxygenation of Lignin Bio-Oil to Hydrocarbons

Jialu Wang, Man Ho Han, Kezia Megagita Gerby Langie, Da Hye Won, Mi-Young Lee, Cheoulwoo Oh, Hyo Sang Jeon, Jai Hyun Koh, Hyung-Suk Oh, Dong Ki Lee, and Woong Hee Lee*



Cite This: *J. Am. Chem. Soc.* 2025, 147, 4962–4971



Read Online

ACCESS |



Metrics & More

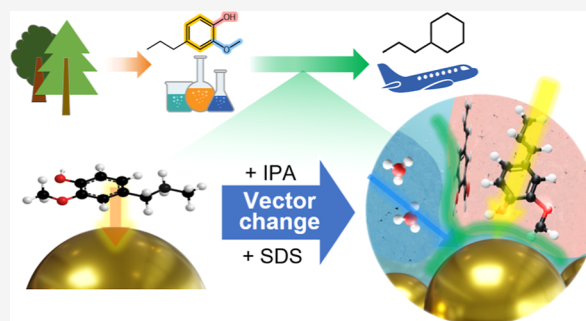


Article Recommendations



Supporting Information

ABSTRACT: Electrocatalytic hydrodeoxygenation (EHDO) is a promising approach for upgrading biomass-derived bio-oils to sustainable fuels without the use of high-pressure hydrogen gas and elevated temperatures. However, direct EHDO for realistic hydrophobic lignin-based oil production remains challenging. Herein, we discuss the molecular dynamics that govern the EHDO of lignin bio-oil over Pt/C in an acidic electrolyte added with 2-propanol or a surfactant. Excellent conversion (98.1%) and a high yield (79.0%) of hydrogenated products, including 40.5% propyl-cyclohexane, are achieved under ambient temperature and pressure. Experimental results and various investigations on molecular dynamics suggest that EHDO occurs at the water-solvent-catalyst three-phase boundary. Proton transfer significantly influences the current density of EHDO. Factors such as cluster size and vector of lignin-based oil to electrode govern the selectivity and Faradaic efficiency of EHDO. This work advances the understanding of dynamics for EHDO and suggests governing factors to improve it.



INTRODUCTION

To meet the increasing global demand for replacing petroleum-based economies and achieving a carbon-neutral society, sustainable energy sources are gaining significant attention.^{1,2} Among the various biomass components, lignin is a promising renewable feedstock to produce liquid fuels and chemicals.^{3,4} The complex 3D structure of lignin, including carbon–oxygen bonds in the phenyl ring, necessitates decomposition processes such as pyrolysis and hydrothermal liquefaction for producing bio-oils.^{5,6} Despite the decomposition process, lignin bio-oil contains oxygenated functional groups, which lead to poor stability and low heat values.^{7,8} Therefore, upgrading bio-oils through hydrodeoxygenation (HDO) is necessary to produce hydrocarbons that can be used as jet fuels.^{9,10} Conventional thermocatalytic HDO is operated under high-pressure hydrogen gas and elevated temperatures. Therefore, accomplishing HDO under low temperature and ambient pressure is a key challenge for realistic lignin-based fuel production.^{11,12}

Electrocatalytic HDO (EHDO) can be a promising approach to remove the functional groups in bio-oils owing to their mild reaction conditions.^{13–15} Recent reports have proposed two types of EHDO methods: direct and indirect methods. For direct EHDO, HDO occurs at the electrode,^{16–18} while proton adsorbed Pt/C nanoparticles serve as the active sites for indirect EHDO, and side reactions, such as hydrogen production or the protonation of chemicals, occur at the electrode for protonation of Pt/C.^{19–21} Recently, highly

efficient indirect EHDO of lignin-based monomers with good hydrocarbon yield was achieved using a combination of a Pt/C catalyst and polyoxometalates.^{19,22,23} Direct EHDO with a small amount of Pt/C, without using expensive polyoxometalates, has the advantage of economic efficiency. Various lignin-oil model compounds have been studied for EHDO using a metal catalyst such as Pt,^{19,21–23} Ru,¹⁸ and Ni.^{24,25} However, the low selectivity and Faradaic efficiency (FE) of direct EHDO remain critical challenges. Furthermore, a real lignin derived bio-oil contains further hydrophobic moieties than the generally studied model compounds, making it difficult to use an aqueous electrolyte system.^{24,26,27} To address these challenges, a detailed discussion of critical descriptors for the EHDO of hydrophobic lignin-derived bio-oils is required.

Herein, we discuss the factors governing the direct EHDO of lignin-based oils to produce hydrocarbon fuels (Figure 1). To simulate real lignin-derived oils, which contain both hydrophilic and hydrophobic moieties, we selected 2-methoxy-4-propylphenol (2M4P) as the main model compound. 2M4P contains a hydrophobic propyl group and three functional

Received: October 10, 2024

Revised: January 13, 2025

Accepted: January 14, 2025

Published: January 21, 2025



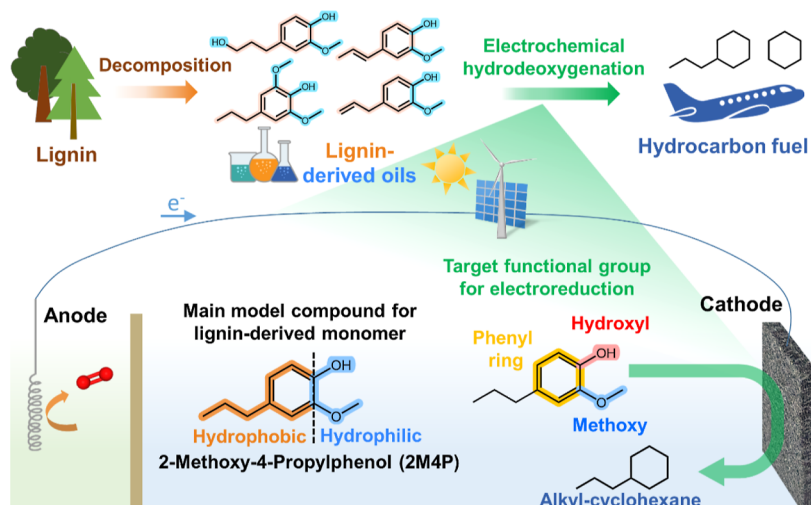


Figure 1. Illustration of the upgradation of lignin-derived oils via EHDO. Lignin-derived oils can be reduced to produce jet fuels through the EHDO approach. 2-Methoxy-4-Propylphenol, a model compound with hydrophobic and hydrophilic moieties, is converted to alkyl-cyclohexane over a Pt/C cathode.

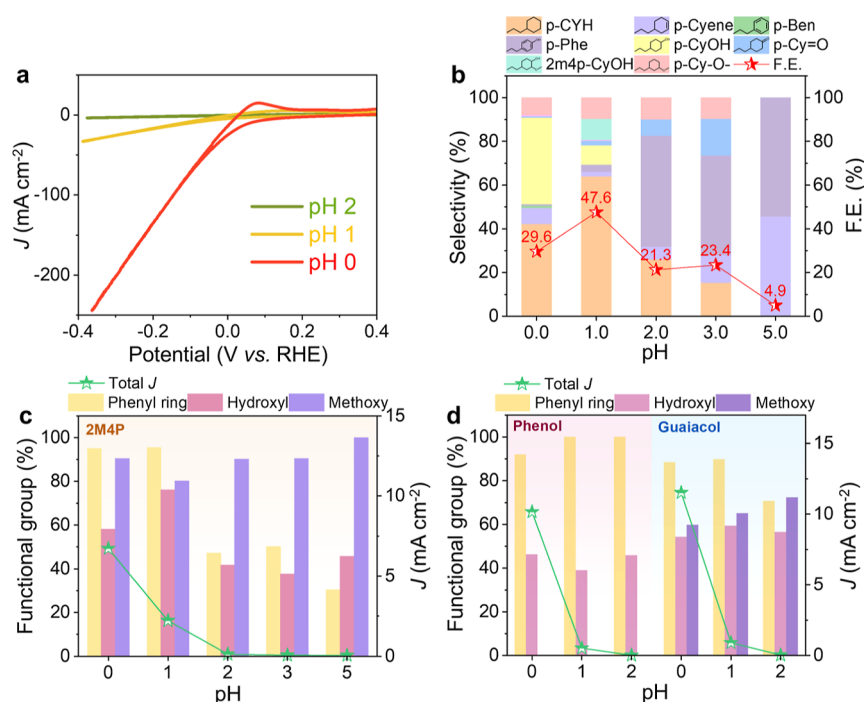


Figure 2. Proton effect on the EHDO of lignin-based oil. (a) Cyclic voltammograms recorded at different pH in 0.1 M HClO₄ with 40% IPA and 10 mM 2M4P (an H-cell with a Nafion 117 membrane and Pt/C-coated carbon felt cathode was used). (b) EHDO of 2M4P at different pH. (c) Calculated hydrogenated functional group ratios and total current densities of 2M4P subjected to EHDO at different pH. (d) Calculated hydrogenated functional group ratios and total current density of phenol and guaiacol subjected to EHDO at different pH.

groups that can be electrochemically reduced: a phenyl ring, a hydroxyl group, and a methoxy group. To elucidate the effect of the hydrophobic group, phenol (without propyl and methoxy groups) and guaiacol (without propyl group) were also studied as models. For electrochemical tests, we used an H-type cell with Pt/C-coated carbon felt as the cathode, a bipolar membrane, and different acidic media on the cathode side (Figures S1–S3). The electrolyte composition, such as the proton concentration, isopropyl alcohol (IPA) ratio, and surfactant, was varied to identify the factors that govern the EHDO of the model compounds. Our analysis suggests that dynamics in the electrolyte, including the hydrogen bond

network, vector of reactants, and cluster size, govern the EHDO of lignin-based oil.

RESULTS AND DISCUSSION

Effect of Proton on the EHDO of Lignin-Based Oil.

EHDO experiments were conducted in a 0.1 M HClO₄ electrolyte with 40% IPA added using a bipolar membrane and Pt/C-coated carbon felt cathode. Considering the poor water solubility of 2M4P, IPA was used for its dissolution in the aqueous electrolyte (Figure S4). After screening several metal candidates, Pt was selected as the electrocatalyst for EHDO owing to its high catalytic selectivity and good stability

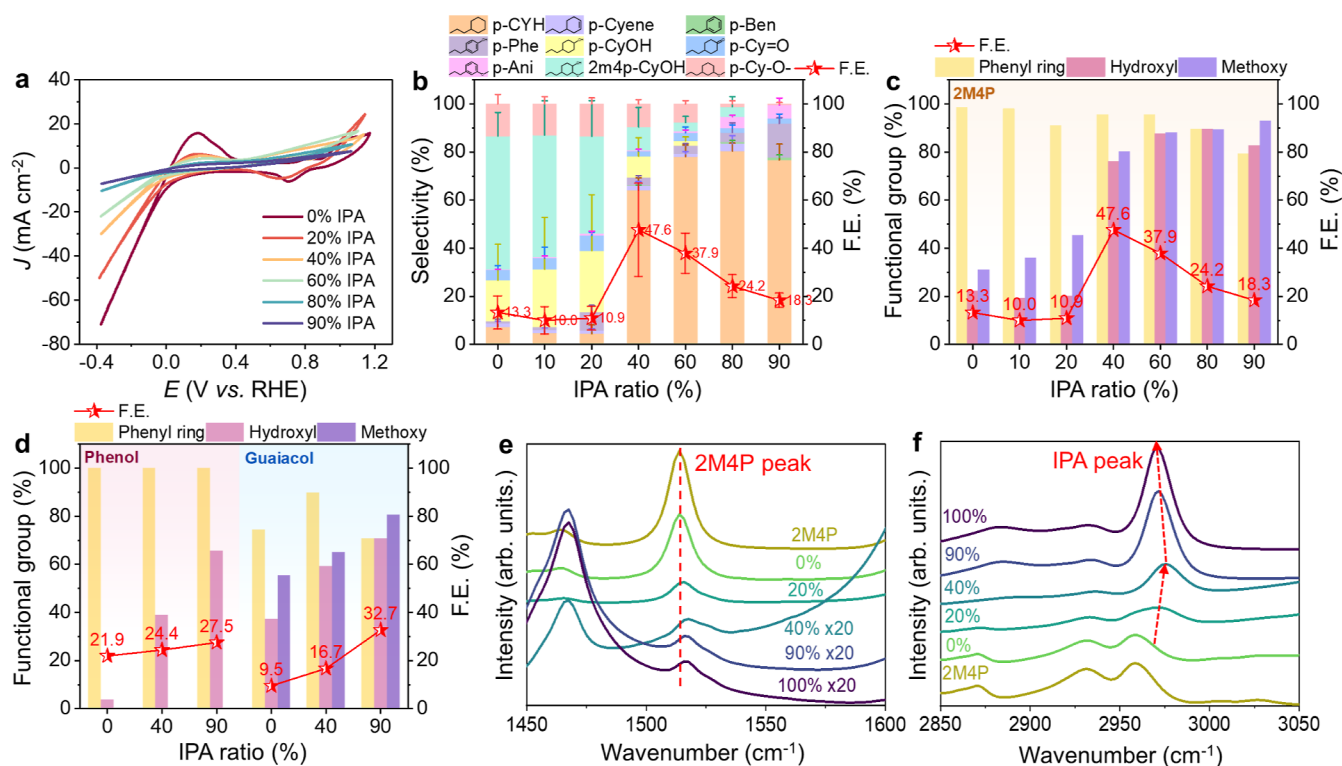


Figure 3. Effect of isopropanol (IPA) on the EHDO of lignin-based oil. (a) Cyclic voltammograms recorded in 0.1 M HClO₄ electrolytes with 10 mM 2M4P and different IPA ratios. (b) EHDO of 2M4P at different IPA ratios. Error bars indicate the standard deviations of three independent measurements. (c) Calculated hydrogenated functional group ratios and FE values for the EHDO of (c) 2M4P and (d) phenol and guaiacol at different IPA ratios. (e,f) ATR-IR spectra of 0.1 M HClO₄ with 100 mM 2M4P and different IPA ratios. Dash lines in (e) and (f) represent the peaks of 2M4P and IPA, respectively.

(Figures S5–S8). An optimal potential of -0.1 V [vs a reversible hydrogen electrode (RHE)] was applied for achieving high FE and avoiding vigorous hydrogen evolution reaction (HER) (Figure S9). To calculate the FE of EHDO, the reaction pathway for the reduction of the methoxy group was elucidated by gas chromatography (GC; Figure S10). Hydrogen was detected due to the occurrence of HER as a side reaction during EHDO. CH₄ was rarely detected, indicating that the methoxy group was reduced to methanol rather than methane and water.

To investigate the role of proton, the EHDO reactions of 2M4P, phenol, and guaiacol were evaluated for 1 h under different pH values (Figures 2 and S11–S13). The current density increased significantly at a high proton concentration, indicating that the proton is the main reactant and hydrogen source for electrochemical reduction (Figure 2a). Figure 2b presents the FE and selectivity for the EHDO of 2M4P. The highest selectivity (62%) for the fully saturated target product, propyl-cyclohexane, was obtained with a satisfactory total FE (47.6%) at pH 1. The ratios of the reduced functional groups of 2M4P at different pH and the corresponding current densities in Figure 2c further illustrate the effects of the proton. Figure 2c clearly suggests that the current density of the system and reduction selectivity of the phenyl ring are predominantly determined by the proton concentration, further verifying that the proton is the highly active reactant in the reduction of the phenyl ring at the Pt/C-coated cathode. The EHDO selectivity of the methoxy group increased marginally with increasing pH, indicating its lower sensitivity to proton. The EHDO selectivities of the phenyl and methoxy moieties of guaiacol followed trends similar to those of 2M4P (Figure 2d).

However, phenol showed a high EHDO selectivity for the phenyl ring in the pH range of 0–2.

Effect of IPA on the EHDO of Lignin-Based Oil. To investigate the EHDO selectivities of different functional groups, reactions were conducted with different IPA ratios and a fixed HClO₄ concentration of 0.1 M (HClO₄ is a strong acid, expecting similar pH values at different IPA ratios). Interestingly, IPA affects not only the solubility of 2M4P but also the HER activity (Figure 3a). As the amount of proton (the HER reactant) is constant, we estimated that HER activity is influenced by not only proton concentration but also proton transfer. This can be inferred that IPA influenced proton transfer. Proton transfer mechanisms in electrolytes can be classified into two types: (i) Grotthuss mechanism involving rapid proton transfer through hydrogen-bonded networks in water and (ii) vehicle mechanism involving the diffusion of protonated species.^{28,29} We anticipated that IPA would break the hydrogen bond network, thereby reducing the current density. As shown in Figures 3b, S14, and S15, both the FE and the EHDO selectivity of 2M4P increased significantly as the IPA ratio increased from 20 to 40%. At >40% IPA, the FE decreased with the increasing IPA ratio. The EHDO selectivities of the hydroxyl and methoxy groups increased with an increasing IPA ratio, whereas that of the phenyl ring decreased (Figure 3c). Similar trends were observed for the EHDO selectivities of phenol and guaiacol (Figures 3d and S16). Interestingly, the FE trend relative to the IPA ratio of phenol and guaiacol differed from that of 2M4P, indicating that the hydrophobicity of the lignin-based oil component affects the FE of EHDO. These results suggest that not only

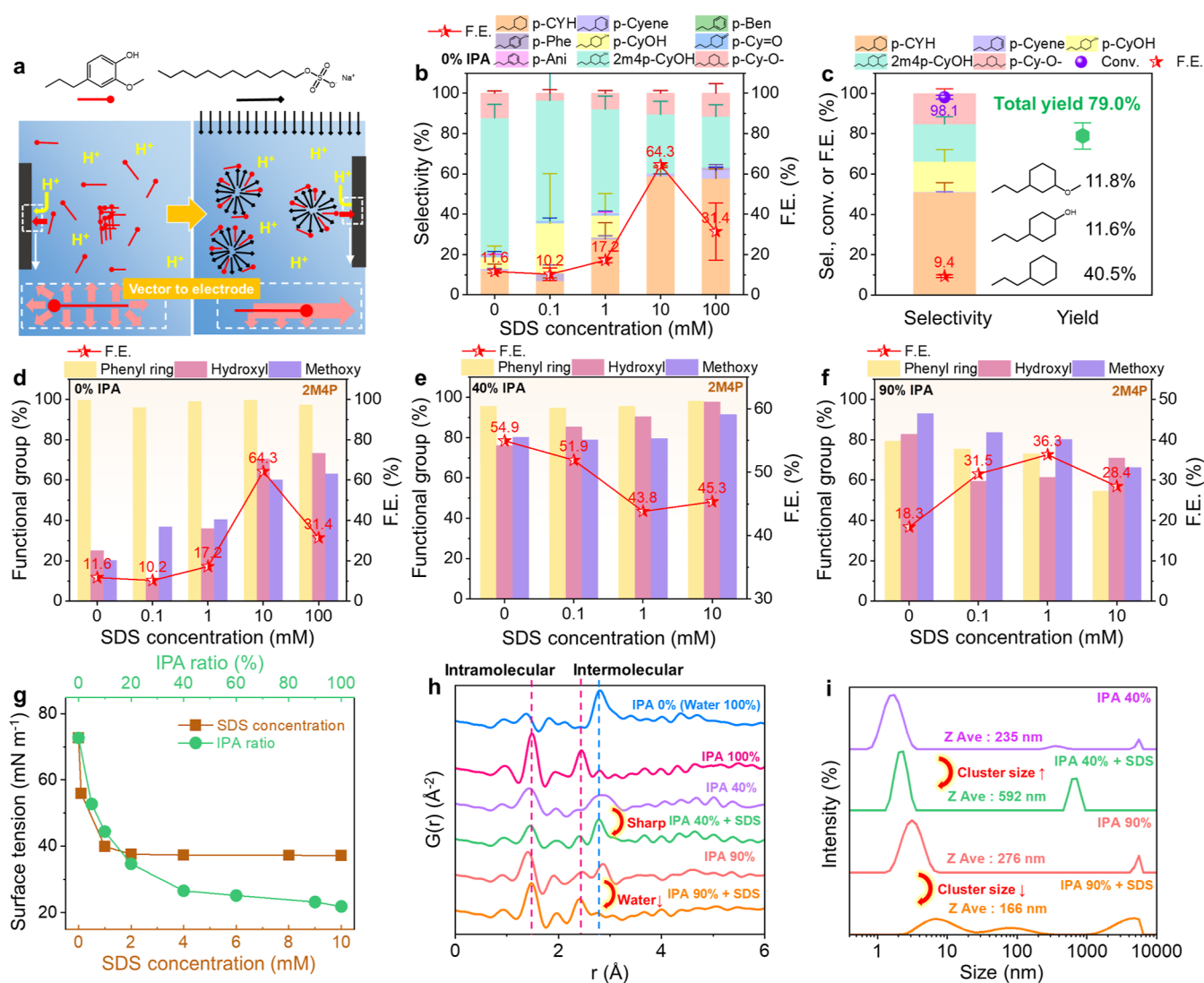


Figure 4. Effect of SDS on the reactant vectors and cluster size of the solvent. (a) Scheme of vectors of 2M4P molecules with respect to the electrode before and after SDS addition in the electrolyte. (b) EHDO of 2M4P at different SDS concentrations. Error bars indicate the standard deviations of three independent measurements. (c) Stability of the EHDO of 2M4P at 10 mM SDS over 24 h and yields of the total and each product. Error bars indicate the standard deviations of five independent measurements. (d–f) Hydrogenated functional group ratios and FE of 2M4P EHDO at different SDS concentrations in 0.1 M HClO₄ solutions with (d) 0%, (e) 40%, and (f) 90% IPA. (g) Surface tensions of 0.1 M HClO₄ solutions with different IPA ratios and SDS concentrations. (h) XPDF and (i) dynamic light scattering analysis of 0.1 M HClO₄ in 90% IPA in the presence and absence of 10 mM SDS.

chemical concentration but also molecular dynamics factor such as **hydrophobicity** part is a key factor for EHDO.

To understand the EHDO trend according to the IPA ratio, attenuated total reflection infrared (ATR-IR) spectra of different electrolytes were obtained by focusing on the bottom fraction of the solution (Figures 3e,f, and S17). In Figure 3e, the peak at 1512 cm⁻¹, corresponding to aromatic C=C in 2M4P, of neat 2M4P is identical to that in an IPA-free electrolyte and slightly shifted at 20% IPA. When the IPA content exceeded 40%, the 2M4P peak weakened and shifted considerably, indicating that 2M4P was completely dissolved at 40% IPA. According to the previous studies on water–alcohol mixtures, molecular dynamics change with the alcohol/water ratio and can be investigated using various spectroscopic techniques.^{30–32} The IR peak at ~2960 cm⁻¹, attributed to the O–H stretching of IPA, shows a red shift below 40% of the IPA ratio and a blue shift above 40% IPA. The reversal of the IPA peak shift at 40% IPA indicates the **phase transition of the**

IPA–water mixture, which significantly changes the EHDO selectivity. This analysis suggests that molecular dynamics in the electrolyte govern the selectivity of EHDO.

Effect of the Reactant Vector and Cluster Size on EHDO. To further control the molecular dynamics of the EHDO system, sodium dodecyl sulfate (SDS), a surfactant, was added to the 0.1 M HClO₄ electrolyte. Several recent studies have reported that the efficiency of electrochemical organic conversion reactions can be enhanced by utilizing surfactants to tune the **reaction microenvironment**.^{33–35} SDS was expected to not only enhance the solubility of 2M4P in 0.1 M HClO₄ without IPA but also change the vector of 2M4P with respect to the electrode (Figure S18). Surfactants such as SDS form micelles when their concentration exceeds the critical micellar concentration.^{36–38} As shown in Figure 4a, in the presence of SDS micelles, 2M4P is expected to be aligned with its hydrophilic domain facing outward and hydrophobic domain (propyl group) positioned inward or parallel to the

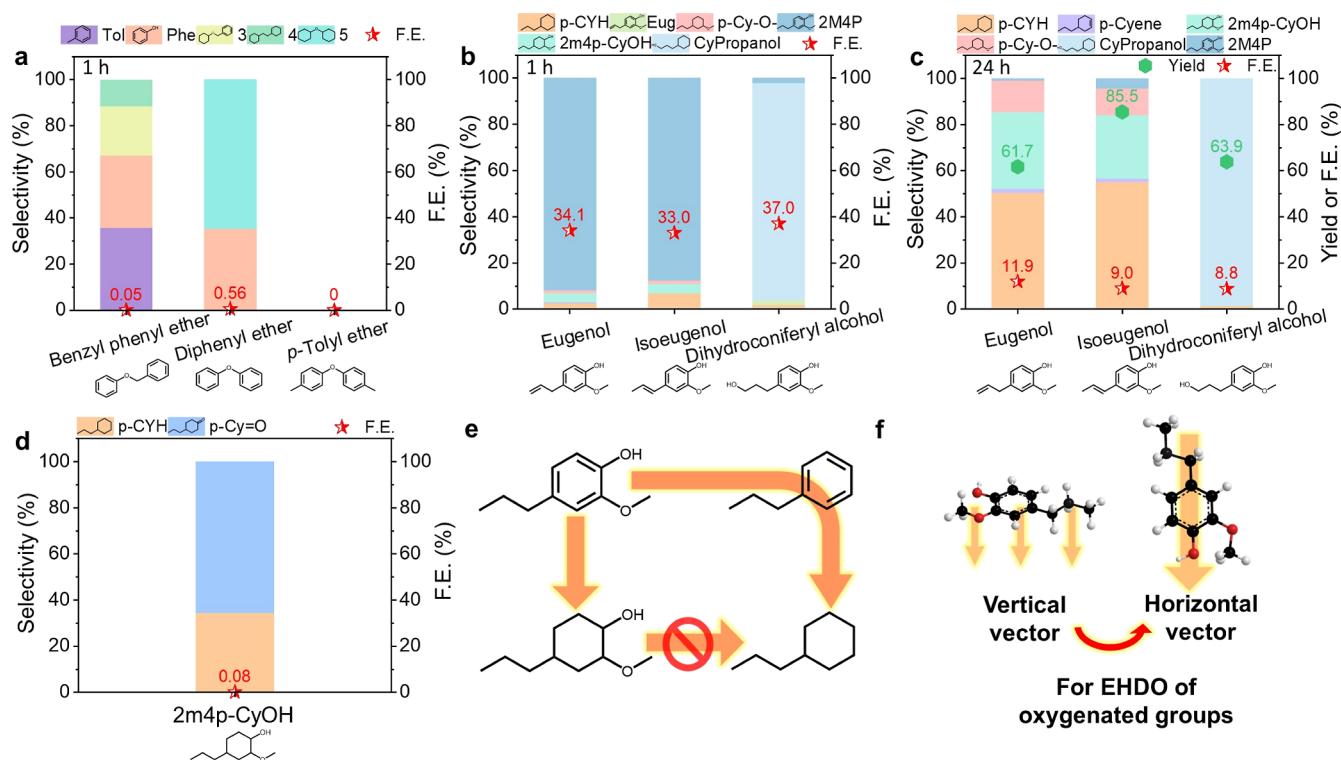


Figure 5. EHDO for converting various functional groups of bio-oils. (a) Results of 1 h EHDO tests of lignin-derived dimers in 0.1 M HClO₄ with 10 mM SDS. Results of (b) 1 h and (c) 24 h EHDO tests of other lignin-derived monomers in the presence of 10 mM SDS. (d) Results of the 1 h EHDO of 2-methoxy-4-propyl-cyclohexanol in the presence of 10 mM SDS. (e) Possible difficult and facile reaction pathways to produce propyl cyclohexane. (f) Illustration of vertical and horizontal vectors of 2M4P molecules toward the electrode for EHDO of oxygenate functional groups.

water-micelle interface.^{38,39} The EHDO FE and selectivity of 2M4P were evaluated at -0.1 V for 1 h at different SDS concentrations in 0.1 M HClO₄ without IPA (Figures 4b, S19, and S20). In this situation, SDS has no significant effect on HER activity at low concentration (below 100 mM) owing to its lower concentration than the IPA experiment (Figure S21). This provides advantages to high current densities and allows focusing on the effects of the reaction vector. The FE and selectivity of the EHDO of 2M4P were substantially improved at SDS concentrations exceeding 1 mM, indicating the positive role of SDS in the EHDO system. However, the FE decreased at 100 mM SDS because the excess SDS impedes the transport of reactants to the electrode. In the 24 h test with 10 mM SDS, the direct EHDO system exhibited 98.1% conversion with a high yield of the hydrogenated products of 79.0%, which includes 40.5% propylcyclohexane (Figures 4c, S22, and S23). The FE of the 24 h test is lower than that of the 1 h test owing to the low reactant concentration (Figure S24), rather than metal leaching in acid and the change of SDS (Figures S25 and S26). This result highlights the feasibility of obtaining a high hydrocarbon yield via the EHDO of the bio-oil under ambient temperature and pressure, in stark contrast with the previous studies on EHDO performed at a high temperature under high H₂ pressure.

Additional EHDO experiments on 2M4P were conducted by varying both the SDS concentration and IPA ratio to analyze the factors governing the FE and selectivity of EHDO (Figures 4d–f, S27 and S28). At 40 and 90% IPA, the reactant was completely soluble in the electrolyte. Thus, in this case, molecular dynamics would be a key factor to determine FE and selectivity of EHDO. At 40% IPA, the FE of EHDO decreased with increasing SDS concentration, whereas it increased with

SDS concentration at 90% IPA. The EHDO selectivities of different functional groups exhibited a reverse trend compared to that of the FE. For comparison, the effect of SDS on the EHDO of guaiacol was also examined (Figure S29). Water-soluble guaiacol showed little difference with SDS addition, indicating that SDS affects the interface of hydrophobic and hydrophilic components in the electrolyte.

To rationalize the trend of EHDO with respect to SDS and IPA factors, various analyses were conducted to comprehend their molecular dynamics of the electrolyte. Surface tension analyses revealed the critical micelle concentration of SDS (1 mM), indicating that the micelles formed at 10 mM SDS concentration orient the 2M4P molecules favorably, leading to high selectivity in EHDO (Figure 4g). X-ray particle distribution function (XPDF) and dynamic light scattering (DLS) analyses of 0.1 M aqueous HClO₄ solutions with different SDS and IPA concentrations were conducted to monitor the distribution of water and IPA clusters in the electrolyte. The electrolyte without IPA (0.1 M HClO₄) provided a clear O–O intermolecular peak, and 100% IPA exhibited C–C and C–O, intramolecular and intermolecular peaks, respectively (Figures 4h and S30). The 0.1 M HClO₄ electrolyte with 40% IPA yielded broad peaks for IPA and water, indicating that the two media were well mixed. When SDS was added to 0.1 M HClO₄ with 40% IPA, the peak shapes of IPA and water sharpened, suggesting that SDS separated the mixed IPA and water phases. However, the water peak of the electrolyte with 90% IPA broadened after the SDS addition. This phenomenon was also observed in DLS studies (Figures 4i and S31). When SDS was added, the average cluster size of the electrolyte with 40% IPA increased, whereas that of the electrolyte with 90% IPA decreased. Interestingly,

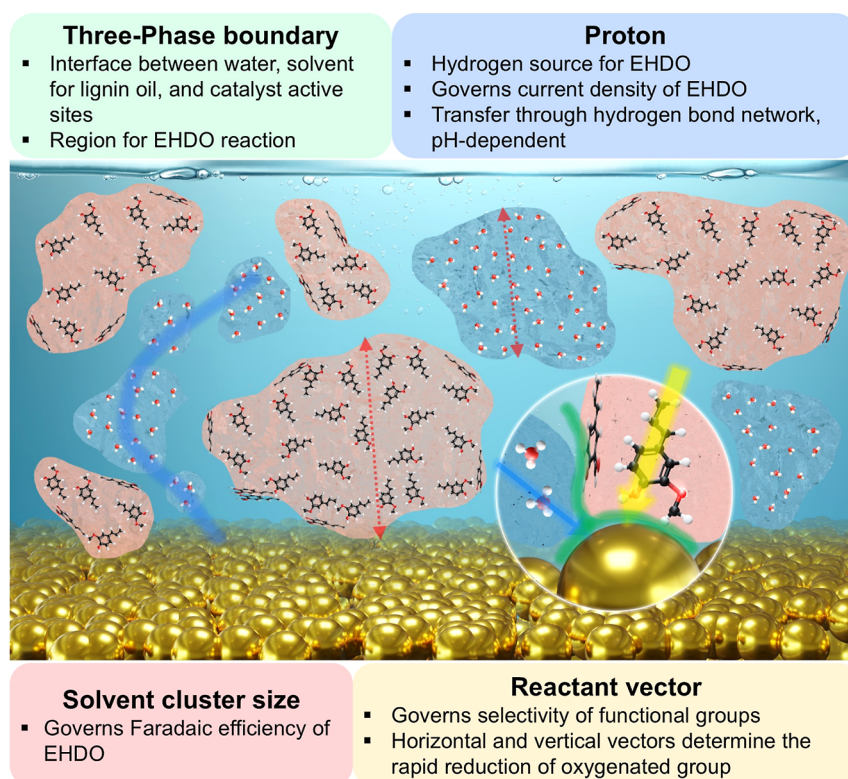


Figure 6. Proposed governing factors related to the molecular dynamics of the electrolyte for EHDO. Scheme of the alignment of the reactant in the electrolyte and the interaction with the catalysts at the three-phase boundary of the reaction system. The illustrations with blue and pink backgrounds in the scheme represent clusters of electrolyte and the solvent for dissolving reactant, respectively. The black, white, and red balls represent carbon, hydrogen, and oxygen atoms, respectively.

these trends are similar to that of the FE of EHDO, implying that the FE is highly influenced by the cluster size of the electrolyte. According to molecular dynamics studies of water/alcohol mixtures, the cluster size of the solvents increases, and the solvent mixing degree decreases as the water or alcohol content is increased. This explains the larger cluster size of the 90% IPA case relative to that of the 40% IPA case.^{30,40,41} The surfactant not only forms micelles that segregate hydrophobic and hydrophilic molecules but also stabilizes immiscible liquids. Based on the XPDF and DLS results, we infer that SDS further separates IPA and water clusters and increases their size in the 40% IPA case. However, SDS distributes the water clusters in large IPA clusters at 90% IPA, decreasing the average cluster size of the electrolyte.

Versatility of EHDO in Converting Various Lignin-Derived Chemicals. The EHDO reactions of other lignin-derived oxygenated molecules were investigated to verify the scalability of the methodology proposed in this study. Dimers, including benzyl phenyl ether, diphenyl ether, and *p*-tolyl ether, which have lower solubility than 2M4P in the electrolyte at 10 mM SDS, owing to their hydrophobic functional groups, exhibited low FEs at 10 mM SDS (Figures 5a and S32). When 40% IPA was added instead of SDS, the FE values of EHDO increased but were still lower than those of 2M4P (Figures S33 and S34). **These results indicate that controlling the vector of the target ether linkage in the dimer is challenging for direct EHDO (Figure S35).**

When EHDO experiments on other monomers, including eugenol, isoeugenol, and dihydroconiferyl alcohol, were conducted at 10 mM SDS (Figures 5b and S36), and eugenol and isoeugenol easily converted to 2M4P, indicating that the

C=C bond is easily hydrogenated under EHDO conditions. After a 24 h test, both eugenol and isoeugenol were completely converted, providing total hydrocarbon yields of 61.7 and 85.5%, respectively, and exhibited product selectivity similar to that of 2M4P (Figures 5c and S37). In contrast, dihydroconiferyl alcohol was converted to cyclohexyl propanol with 98% selectivity. The electrolytes added with IPA and IPA/SDS also exhibited low selectivity for propyl-cyclohexane, suggesting that the low reducibility of the propyl hydroxyl group is not the vector problem (Figure S38). This phenomenon was also observed in the EHDO of 2-methoxy-4-propyl-cyclohexanol (Figure 5d). **Hydroxyl and methoxy groups attached to the cyclohexane ring were rarely reduced by EHDO, indicating that oxygenated groups such as hydroxyl and methoxy groups linked to a C–C single bond resist electroreduction compared to those linked to C=C bonds or phenyl rings (Figure S39).** **These results indicate that the hydroxyl and methoxy groups on a phenyl ring can be reduced before the reduction of the phenyl ring itself (Figure 5e).** The low selectivity at high proton concentrations and low IPA and SDS concentrations can be explained by the rapid electroreduction of phenyl ring. Therefore, we propose that vector-controlled direct EHDO is a crucial strategy for the electroreduction of oxygenated groups (Figure 5f). Roke et al. reported that SDS in a water/oil mixture can be disordered and partially oriented vertically, rather than horizontally with respect to water, which is the normally expected arrangement.³⁶ Thus, lignin-based chemicals, such as 2M4P, can possess both horizontal and vertical vectors to the electrode. The vertical vector of the reactant allows the reduction of both oxygenated functional groups and hydrophobic moieties, such as the phenyl ring and C=C bond

on the alkyl chain. The horizontal vector of the reactant is expected to be more favorable for the reduction of oxygenated functional groups, such as hydroxyl and methoxy functional groups. The **high magnitude of the horizontal vector** for chemicals ensures that oxygenated groups contact the catalyst more quickly and efficiently than the phenyl group, potentially enhancing the selectivity and FE of EHDO.

DISCUSSION OF KEY GOVERNING FACTORS FOR EHDO

From the experimental EHDO results obtained by adding IPA and SDS to the acidic solution, we propose the factors that govern the efficiency of the direct EHDO of a lignin-based oil containing both hydrophilic and hydrophobic components (Figure 6). It is clear that proton is the main hydrogen source for the EHDO and lignin-based chemicals with hydrophobic parts dissolve in IPA or SDS component. Thus, the EHDO reaction would mainly occur at three-phase boundaries between the proton conductive electrolyte (water phase), solvent used for reactant such as lignin oil, and active catalyst sites. We speculate that the formation of this interface is highly dependent on molecular dynamics in the electrolyte.

Hydrogen bond network providing rapid proton transfer is related to the connection of water clusters and governs the current density of EHDO system.^{42,43} The cluster sizes of water and the solvent used for lignin-based oil govern the proportion of the three-phase boundary in the electrolyte. A reduced cluster size increases the interfacial area of each cluster, increasing the possibility of contact with a catalyst site, thereby enhancing the FE of the EHDO. EHDO results for the selectivity of functional groups indicate that proton adsorbed Pt/C sites are highly active for the electroreduction of the phenyl ring. The other governing factor for EHDO of other functional groups is expected to be the reactant vector in the solvent. The ideal solvent for hydrophobic chemicals would push the hydrophilic part of the reactant molecule toward the interface with water, which is the target of EHDO. This would be the origin of the reactant vector with respect to the electrode and governs the FE and selectivity of EHDO by determining the location and arrangement of reactants in the electrolyte.

To understand the EHDO selectivities of different functional groups, horizontal and vertical vectors should be considered for various lignin-based chemicals. To estimate the horizontal vector for each condition, we investigated the FE for the reduction of the C=C bond in eugenol (Figure S40). We suppose that the low FE for eugenol represents a higher horizontal vector than a higher horizontal vector. A high content of IPA or SDS in the electrolyte would enhance the horizontal vector of reactant by rearranging it, leading to a relatively high EHDO for oxygenated functional groups. However, it would also increase the solvent cluster size and break the hydrogen bond network, reducing the FE and current density of the EHDO. Therefore, the EHDO system should be optimized by considering the molecular dynamics in the electrolyte. This discussion provides an understanding of how various factors of molecular dynamics affect EHDO and is expected to facilitate the design of EHDO systems tailored to various target chemicals.

CONCLUSIONS

We discussed key descriptors that affect the performance of direct EHDO of lignin-based oil, such as the current density, FE, and reduction selectivity of various functional groups. A heterogeneous H-type electrochemical system with a HClO₄ solution, bipolar membrane, Pt/C-coated carbon felt cathode, and IPA (and/or SDS) additive was used to investigate the EHDO of 2M4P selected as the main model of lignin-based oil. When 10 mM SDS was introduced into the 0.1 M HClO₄ electrolyte, 64.3% FE and 58.9% selectivities to propyl-cyclohexane were achieved in a 1 h test, while 98.1% conversion with a high yield of total hydrogenated products (79.0%), which includes 40.5% propyl-cyclohexane, was achieved in a 24 h test. According to experimental results and characterization, we suggest that EHDO occurs at three-phase boundaries between the proton conductive electrolyte (such as aqueous HClO₄), the solvent used for reactant dissolution (such as IPA), and the catalyst active sites. The three-phase boundaries depend on the governing factors related to molecular dynamics. Factors that affect the transfer of proton as a main hydrogen source for EHDO reaction, such as proton concentration and hydrogen bond network, determine the current density of EHDO system. The cluster size of water and solvent used for reactant dissolution affects the formation of three-phase boundary, influencing the FE of EHDO. The reactant vectors, including horizontal and vertical vectors, govern the selectivity of various functional groups for EHDO. Oxygenated functional groups on the phenyl ring can be reduced before the phenyl ring itself is reduced, and the horizontal vector of the reactant is expected to be more favorable for reducing oxygenated functional groups. These findings improve the understanding of EHDO system from the viewpoint of molecular dynamics and provide valuable insights into designing electrocatalytic organic conversion systems.

EXPERIMENTAL SECTION

Preparation of Electrodes. Typically, 6.0 mg of Pt/C and 10 μ L of a 5 wt % polytetrafluoroethylene solution were added to an IPA/deionized (DI) water mixture (1:1, v/v), and the resulting mixture was sonicated for 15 min using an ultrasonic processor (VCX 500, Sonics & Materials) equipped with a 6 mm tip to prepare a homogeneous suspension. Sonication was performed at an amplitude of 40% and a pulse of 20 s and 10 s. Then, the suspension was drop-casted on carbon felt (1.5 cm \times 2.0 cm) to form a uniform layer of Pt/C with 2.0 mg cm⁻² loading and dried in air overnight. The obtained electrode is listed as Pt/C-CF.

Other catalysts were synthesized via an electrodeposition method using a 3-electrode system in a 0.5 M Na₂SO₄ solution containing 10 mM relevant metal precursors (Supporting Information and Chemicals). Two pieces of carbon paper were employed as the working and counter electrodes, and Ag/AgCl was used as the reference electrode. Cyclic voltammetry (CV) was conducted for metal deposition in the voltage range of -0.5 to +1.7 V at a scan rate of 100 mV s⁻¹ for 50 cycles. Then, the carbon paper was rinsed with DI water and dried in the air. The obtained material is noted as ed-M-CP (including ed-Pt-CP, ed-Rh-CP, ed-Ni-CP, ed-Au-CP, ed-Ir-CP, ed-Co-CP, ed-Fe-CP, ed-Ag-CP, ed-W-CP, ed-Mg-CP, ed-Pd-CP, and ed-Ru-CP).

EHDO Experiments. An H-cell composed of three electrodes was used for the EHDO experiments. A bipolar membrane was used to prevent the crossover of the organic solvent along with chemicals (Figure S41). 40 mL portion of HClO₄ solution with additives (such as IPA and/or SDS) and 40 mL of 0.1 M NaOH solution were applied as the catholyte and anolyte, respectively. The catalyst-coated carbon felt was used as the working electrode, and a platinum wire

and Ag/AgCl were employed as counter and reference electrodes, respectively. Electrochemical tests were performed using a potentiostat (VSP-3e, BioLogic). For all EHDO tests, the initial reactant concentration was set as 10 mM, unless otherwise specified. Continuous stirring at 600 rpm was performed at the cathode side before and during every test to ensure the homogeneous distribution of electrolyte components and minimize mass transfer limitation. All the measured potentials, E_{measured} , were calibrated to that of the RHE, E_{RHE} , according to the following equation

$$E_{\text{RHE}} = E_{\text{measured}} + 0.0591 \times \text{pH} + E_{\text{Ag/AgCl}} \quad (1)$$

The pH was measured with a pH meter (Mettler-Toledo S220), and $E_{\text{Ag/AgCl}}$ is 0.197.

For CV tests, argon (99.9999%) was purged for 30 min into the cathode solution before measurements, and a Nafion 117 membrane was employed. The CV scan rate was 5 mV s⁻¹ and all results were compensated at 85%, as shown below

$$E_{\text{compensated}} = E_{\text{RHE}} - iR \times 85\% \quad (2)$$

where the E_{RHE} is the potential calibrated via Formula 1, i is the real current value, and R is Ohmic resistance measured by potentiometric electrochemical impedance spectroscopy (PEIS) technique with various electrolytes (-0.1 V vs RHE was set as the working potential for each PEIS test).

Products Analysis. The liquid products were analyzed by GC combined with mass spectrometry (GC-MS). Typically, an aliquot of the cathode electrolyte was collected during or after electrochemical measurements, and 1.0 mL of the electrolyte was diluted to twice the volume with a mixture of IPA and DI water (1:1, v/v). Subsequently, 1.0 mL of dichloromethane with 10 mM pentadecane as an internal standard was added for extraction. After the mixture was shaken vigorously, it stood undisturbed to allow phase separation. Then, 0.4 mL of the lower organic layer was transferred to another vial and diluted with 1.0 mL of dichloromethane. Thereafter, an appropriate amount of anhydrous sodium sulfate was added to remove the residual water. Finally, the sample was filtered and transferred to an autosampler specialized vial using a syringe. The GC instrument (8890, Agilent) was equipped with an HP-5 ms UI (30 m × 0.25 mm × 0.25 μm) GC column, a mass selective detector (5977B, Agilent), and an autosampler (7693A, Agilent). Helium (99.9999%) was used as the carrier gas. Injection and detector temperatures were set as 250 °C, and the oven temperature was programmed as follows: 40 °C for 0.1 min, ramp to 150 °C at 30 °C min⁻¹ and then to 250 °C at 10 °C min⁻¹, and maintain at 250 °C for 4 min. The products were confirmed by both mass spectroscopy and comparison with standard chemicals. In detail, the peaks of each sample were searched in the library, and the mass spectra were carefully compared with the database. When there were no corresponding chemicals in the database, we compared the retention time and mass spectra with those of standard chemicals. When there were no standard chemicals, we analyzed the unknown product's mass spectra and identified the possible fractions and also compared them with similar chemicals.

The quantitative results were calibrated by the response factor to the internal standard, pentadecane. To determine the response factor of every chemical versus internal standard, 1, 5, and 10 mM standard chemicals were added to 0.1 M aq. HClO₄ solutions with 50% IPA (v/v). Then, the solutions with standard chemicals were treated and analyzed by using the same procedure used for experimental samples, as described above. The raw GC chromatogram for standard chemicals and internal standards are shown in Figure S42. Further, in Figure S43, the corresponding integrated area for each chemical with increasing concentration is drawn with variance values near 1, demonstrating the linear correlation between the peak area and concentration and proving the reliability of using a response factor under different concentrations. Subsequently, the response factor of each chemical was calculated as follows

$$f_p = \frac{A_p \times n_p}{A_s \times n_s} \quad (3)$$

where f_p is the response factor of product p , A_p is the peak area of product p , n_p is the amount of product p , A_s is the peak area of the standard chemical, and n_s is the amount of the standard chemical. Then, the average value of each chemical at different concentrations was calculated and considered as the final response factor. The following relationship was used for quantitative analysis

$$n_p = f_p \times A_p \quad (4)$$

For the products without standard reagents, the response factor was calculated using the same response factor of the similar-structure chemicals (such as using the response factor of 4-propyl-anisole, propyl-cyclohexane, methoxy-cyclohexane for quantitative analysis of 3-propyl-anisole, propyl-cyclohexene, 3-propyl-methoxy-cyclohexane, respectively). The selectivity of each product (S_p), the reactant conversion rate (C), total FE, and the yield of each product (Y_p) were calculated as follows

$$S_p = \frac{n_p}{\sum n_p} \times 100\% \quad (5)$$

$$C = \frac{\sum n_p}{\sum n_p + n_r} \times 100\% \quad (6)$$

$$\text{FE} = \frac{n_p \times C \times F \times \sum (z_p \times S_p)}{\sum (i \times t)} \times 100\% \quad (7)$$

$$Y_p = \frac{n_p}{n_0} \times 100\% \quad (8)$$

where n_r is the reactant amount, n_0 is the initial reactant amount, F is the Faraday constant (96,485 C mol⁻¹), z_p is the electron transfer number for the formation of each product p , and i and t are the reaction current and time, respectively. The total J was calculated from the FE and the current density at 1800 s, J_m , as follows

$$\text{Total } J = \text{FE} \times J_m \quad (9)$$

The gaseous products were detected by GC (Agilent 7890A). The inlet of the GC instrument was directly connected to the cathode outlet. Argon (99.9999%) was used as the carrier gas. The GC instrument was equipped with a thermal conductivity detector (TCD) for H₂ detection and a flame ionization detector (FID) for detecting other gases. MolSieve 5A (6 ft, Agilent) and Porapak Q (13 ft, Agilent) columns were used for the FID and TCD, respectively. Gas samples were collected and analyzed 5 and 30 min after the chronoamperometry reaction. The FE of the gas product was calculated as follows

$$\text{FE} = \frac{i_p}{i_{\text{total}}} \times 100\% = \frac{V_p \times Q \times \frac{z_p \times P \times F}{R \times T}}{i_{\text{total}}} \times 100\% \quad (10)$$

where i_p is the partial current of product p , i_{total} is the total current, V_p is the volume fraction of product p , Q is the flow rate, P is atmospheric pressure (101.325 kPa), R is the ideal gas constant (8.314 J mol⁻¹ K⁻¹), and T is temperature (298 K).

■ ASSOCIATED CONTENT

Supporting Information

The Supporting Information is available free of charge at <https://pubs.acs.org/doi/10.1021/jacs.4c14254>.

Materials and chemicals, physical characterizations, electrolyte characterizations, photos of Pt/C-CF electrode, SEM images of Pt/C-CF electrode, TEM images of Pt/C, photo of 2M4P solubility, products selectivity of 2M4P EHDO, TEM images of Pt/C after reaction, XPS spectra of Pt/C before and after reaction, proton factor of phenol EHDO, IPA factor of 2M4P EHDO, IPA factor of phenol and guaiacol EHDO, ATR-IR

spectra of comparison samples and different IPA ratios, potential factor with SDS of 2M4P EHDO, SDS factor of 2M4P EHDO, CV and LSV curves, CA curves of 2M4P EHDO stability tests, 2M4P EHDO stability tests, reactant concentration factor, recyclability tests of Pt/C-CF, SDS peaks in GC spectra, 2M4P EHDO with SDS and 40% IPA, guaicol EHDO with 90% IPA, XPDF results, DLS results, dimers EHDO, CA curves of dimers EHDO, products selectivity, yield, and FE of dimers EHDO, scheme of *p*-tolyl ether vector, other monomers EHDO, dihydroconiferyl alcohol EHDO, reduction difficulty extent, products selectivity and FE of eugenol EHDO, anolyte comparison, GC-MS spectra of standard chemicals, and integrated peak area of standard chemicals(PDF)

AUTHOR INFORMATION

Corresponding Author

Woong Hee Lee – Clean Energy Research Center, Korea Institute of Science and Technology (KIST), Seoul 02792, Republic of Korea; Division of Energy and Environmental Technology, KIST School, Korea University of Science and Technology (UST), Seoul 02792, Republic of Korea; orcid.org/0000-0002-5779-3246; Email: abcabac@kist.re.kr

Authors

Jialu Wang – Clean Energy Research Center, Korea Institute of Science and Technology (KIST), Seoul 02792, Republic of Korea

Man Ho Han – Clean Energy Research Center, Korea Institute of Science and Technology (KIST), Seoul 02792, Republic of Korea

Kezia Megagita Gerby Langie – Clean Energy Research Center, Korea Institute of Science and Technology (KIST), Seoul 02792, Republic of Korea; Department of Chemistry, Kookmin University, Seoul 02707, Republic of Korea

Da Hye Won – Clean Energy Research Center, Korea Institute of Science and Technology (KIST), Seoul 02792, Republic of Korea; Division of Energy and Environmental Technology, KIST School, Korea University of Science and Technology (UST), Seoul 02792, Republic of Korea; KHU-KIST Department of Converging Science and Technology, Kyung Hee University, Seoul 02477, Republic of Korea; orcid.org/0000-0002-7589-7866

Mi-Young Lee – Clean Energy Research Center, Korea Institute of Science and Technology (KIST), Seoul 02792, Republic of Korea; orcid.org/0000-0003-1323-7691

Cheoulwoo Oh – Clean Energy Research Center, Korea Institute of Science and Technology (KIST), Seoul 02792, Republic of Korea

Hyoo Sang Jeon – Technological Convergence Center, Korea Institute of Science and Technology (KIST), Seoul 02792, The Republic of Korea; orcid.org/0000-0003-3486-0589

Jai Hyun Koh – Clean Energy Research Center, Korea Institute of Science and Technology (KIST), Seoul 02792, Republic of Korea; Division of Energy and Environmental Technology, KIST School, Korea University of Science and Technology (UST), Seoul 02792, Republic of Korea; orcid.org/0000-0003-2589-8032

Hyung-Suk Oh – Clean Energy Research Center, Korea Institute of Science and Technology (KIST), Seoul 02792, Republic of Korea; KIST-SKKU Carbon-Neutral Research

Center, Sungkyunkwan University 2066 Seobu-ro, Suwon 16419, Republic of Korea; School of Advanced Materials Science & Engineering, Sungkyunkwan University (SKKU), Suwon 16419, Republic of Korea; orcid.org/0000-0002-0310-6666

Dong Ki Lee – Clean Energy Research Center, Korea Institute of Science and Technology (KIST), Seoul 02792, Republic of Korea; Division of Energy and Environmental Technology, KIST School, Korea University of Science and Technology (UST), Seoul 02792, Republic of Korea; Graduate School of Energy and Environment, Korea University, Seoul 02841, Republic of Korea; Department of Chemical and Biomolecular Engineering, Yonsei-KIST Convergence, Research Institute, Yonsei University, Seoul 03722, Republic of Korea; orcid.org/0000-0002-3740-0986

Complete contact information is available at:

<https://pubs.acs.org/10.1021/jacs.4c14254>

Notes

The authors declare no competing financial interest.

ACKNOWLEDGMENTS

This research was supported by the National Research Foundation of Korea (NRF) grant funded by the Ministry of Science and ICT. (project nos: 2022M3A9F3082336 and RS-2024-00431568). We are grateful to institutional program grants from the Korea Institute of Science and Technology.

REFERENCES

- (1) Schutyser, W.; Renders, T.; Van den Bosch, S.; Koelewijn, S. F.; Beckham, G. T.; Sels, B. F. Chemicals from lignin: an interplay of lignocellulose fractionation, depolymerisation, and upgrading. *Chem. Soc. Rev.* **2018**, *47*, 852–908.
- (2) Tian, C.; Dorakhan, R.; Wicks, J.; Chen, Z.; Choi, K.-S.; Singh, N.; Schaidle, J. A.; Holewinski, A.; Vojvodic, A.; Vlachos, D. G.; Broadbelt, L. J.; Sargent, E. H. Progress and roadmap for electro-privileged transformations of bio-derived molecules. *Nat. Catal.* **2024**, *7*, 350–360.
- (3) Du, X.; Zhang, H.; Sullivan, K. P.; Gogoi, P.; Deng, Y. Electrochemical lignin conversion. *ChemSusChem* **2020**, *13*, 4318–4343.
- (4) Li, C.; Zhao, X.; Wang, A.; Huber, G. W.; Zhang, T. Catalytic transformation of lignin for the production of chemicals and fuels. *Chem. Rev.* **2015**, *115*, 11559–11624.
- (5) Besson, M.; Gallezot, P.; Pinel, C. Conversion of biomass into chemicals over metal catalysts. *Chem. Rev.* **2014**, *114*, 1827–1870.
- (6) Sun, Z.; Fridrich, B.; de Santi, A.; Elangovan, S.; Barta, K. Bright side of lignin depolymerization: toward new platform chemicals. *Chem. Rev.* **2018**, *118*, 614–678.
- (7) Liu, G.; Robertson, A. W.; Li, M. M.-J.; Kuo, W. C. H.; Darby, M. T.; Muhieddine, M. H.; Lin, Y.-C.; Suenaga, K.; Stamatakis, M.; Warner, J. H.; Tsang, S. C. E. MoS₂ monolayer catalyst doped with isolated Co atoms for the hydrodeoxygenation reaction. *Nat. Chem.* **2017**, *9*, 810–816.
- (8) Lee, H.; Kim, H.; Yu, M. J.; Ko, C. H.; Jeon, J. K.; Jae, J.; Park, S. H.; Jung, S. C.; Park, Y. K. Catalytic hydrodeoxygenation of bio-oil model compounds over Pt/HY catalyst. *Sci. Rep.* **2016**, *6*, 28765.
- (9) Duan, H.; Dong, J.; Gu, X.; Peng, Y.-K.; Chen, W.; Issariyakul, T.; Myers, W. K.; Li, M.-J.; Yi, N.; Kilpatrick, A. F. R.; Wang, Y.; Zheng, X.; Ji, S.; Wang, Q.; Feng, J.; Chen, D.; Li, Y.; Buffet, J.-C.; Liu, H.; Tsang, S. C. E.; O'Hare, D. Hydrodeoxygenation of water-insoluble bio-oil to alkanes using a highly dispersed Pd-Mo catalyst. *Nat. Commun.* **2017**, *8*, 591.
- (10) Duan, H.; Liu, J.-C.; Xu, M.; Zhao, Y.; Ma, X.-L.; Dong, J.; Zheng, X.; Zheng, J.; Allen, C. S.; Danaie, M.; Peng, Y.-K.; Issariyakul, T.; Chen, D.; Kirkland, A. I.; Buffet, J.-C.; Li, J.; Tsang, S. C. E.;

O'Hare, D. Molecular nitrogen promotes catalytic hydrodeoxygenation. *Nat. Catal.* **2019**, *2*, 1078–1087.

(11) Liu, W.; You, W.; Sun, W.; Yang, W.; Korde, A.; Gong, Y.; Deng, Y. Ambient-pressure and low-temperature upgrading of lignin bio-oil to hydrocarbons using a hydrogen buffer catalytic system. *Nat. Energy* **2020**, *5*, 759–767.

(12) Yang, Z.; Luo, B.; Shu, R.; Zhong, Z.; Tian, Z.; Wang, C.; Chen, Y. Synergistic effect of active metal–acid sites on hydrodeoxygenation of lignin-derived phenolic compounds under mild conditions using Ru/C-HPW catalyst. *Fuel* **2022**, *319*, 123617.

(13) Akhade, S. A.; Singh, N.; Gutierrez, O. Y.; Lopez-Ruiz, J.; Wang, H.; Holladay, J. D.; Liu, Y.; Karkamkar, A.; Weber, R. S.; Padmaperuma, A. B.; Lee, M.-S.; Whyatt, G. A.; Elliott, M.; Holladay, J. E.; Male, J. L.; Lercher, J. A.; Rousseau, R.; Glezakou, V.-A. Electrocatalytic hydrogenation of biomass-derived organics: A review. *Chem. Rev.* **2020**, *120*, 11370–11419.

(14) Wong, S. S.; Shu, R.; Zhang, J.; Liu, H.; Yan, N. Downstream processing of lignin derived feedstock into end products. *Chem. Soc. Rev.* **2020**, *49*, 5510–5560.

(15) Wijaya, Y. P.; Smith, K. J.; Kim, C. S.; Gyenge, E. L. Electrocatalytic hydrogenation and depolymerization pathways for lignin valorization: toward mild synthesis of chemicals and fuels from biomass. *Green Chem.* **2020**, *22*, 7233–7264.

(16) Peng, T.; Zhuang, T.; Yan, Y.; Qian, J.; Dick, G. R.; de Behaghel, J.; Peng, T.; Zhuang, T.; Yan, Y.; Wang, Z.; Dick, G. R.; Behaghel de Bueren, J.; Qian, J.; Zhang, Y.; Wang, Z.; Wicks, J.; Garcia de Arquer, F. P.; Abed, J.; Wang, Z.; Sedighian Rasouli, A.; Lee, G.; Wang, M.; Wang, N.; Wang, Z.; Liang, Z.; Song, L.; Wang, X.; Chen, B.; Ozden, A.; Lum, Y.; Leow, W. R.; Luo, M.; et al. Ternary alloys enable efficient production of methoxylated chemicals via selective electrocatalytic hydrogenation of lignin monomers. *J. Am. Chem. Soc.* **2021**, *143*, 17226–17235.

(17) Zhou, Y.; Gao, Y.; Zhong, X.; Jiang, W.; Liang, Y.; Niu, P.; Li, M.; Zhuang, G.; Li, X.; Wang, J. Electrocatalytic upgrading of lignin-derived bio-oil based on surface-engineered PtNiB nanostructure. *Adv. Funct. Mater.* **2019**, *29*, 1807651.

(18) Garedew, M.; Young-Farhat, D.; Jackson, J. E.; Saffron, C. M. Electrocatalytic upgrading of phenolic compounds observed after lignin pyrolysis. *ACS Sustain. Chem. Eng.* **2019**, *7*, 8375–8386.

(19) Liu, W.; You, W.; Gong, Y.; Deng, Y. High-efficiency electrochemical hydrodeoxygenation of bio-phenols to hydrocarbon fuels by a superacid-noble metal particle dual-catalyst system. *Energy Environ. Sci.* **2020**, *13*, 917–927.

(20) Wijaya, Y. P.; Grossmann-Neuhaeusler, T.; Dhewangga Putra, R. D.; Smith, K. J.; Kim, C. S.; Gyenge, E. L. Electrocatalytic hydrogenation of guaiacol in diverse electrolytes using a stirred slurry reactor. *ChemSusChem* **2020**, *13*, 629–639.

(21) Wijaya, Y. P.; Smith, K. J.; Kim, C. S.; Gyenge, E. L. Hydrodeoxygenation of lignin related phenolic monomers in polar organic electrolyte via electrocatalysis in a stirred slurry catalytic reactor. *Green Chem.* **2022**, *24*, 7469–7480.

(22) Han, S.; Zhang, X.; Wang, R.; Wang, K.; Jiang, J.; Xu, J. Electrocatalytic conversion of G-type and S-type phenolic compounds from different tree species in a heteropolyacid fluidized system. *Chem. Eng. J.* **2023**, *452*, 139299.

(23) Zhai, Q.; Han, S.; Hse, C.-Y.; Jiang, J.; Xu, J. Electrocatalytic hydrogenation of mono- and dimeric lignin to hydrocarbons in fluidized electrocatalytic system. *Fuel Process. Technol.* **2022**, *227*, 107109.

(24) Zhou, Y.; Klinger, G. E.; Hegg, E. L.; Saffron, C. M.; Jackson, J. E. Multiple mechanisms mapped in aryl alkyl ether cleavage via aqueous electrocatalytic hydrogenation over skeletal nickel. *J. Am. Chem. Soc.* **2020**, *142*, 4037–4050.

(25) Ilikti, H.; Reki, N.; Thomalla, M. Electrocatalytic hydrogenation of phenol in aqueous solutions at a Raney nickel electrode in the presence of cationic surfactants. *J. Appl. Electrochem.* **2002**, *32*, 603–609.

(26) Xu, L.; Cao, M.; Zhou, J.; Pang, Y.; Li, Z.; Yang, D.; Leu, S. Y.; Lou, H.; Pan, X.; Qiu, X. Aqueous amine enables sustainable

monosaccharide, monophenol, and pyridine base coproduction in lignocellulosic biorefineries. *Nat. Commun.* **2024**, *15*, 734.

(27) Soares, B.; Tavares, D. J. P.; Amaral, J. L.; Silvestre, A. J. D.; Freire, C. S. R.; Coutinho, J. A. P. Enhanced solubility of lignin monomeric model compounds and technical lignins in aqueous solutions of deep eutectic solvents. *ACS Sustain. Chem. Eng.* **2017**, *5*, 4056–4065.

(28) Agmon, N. The Grothuss mechanism. *Chem. Phys. Lett.* **1995**, *244*, 456–462.

(29) Kreuer, K. D.; Rabenau, A.; Weppner, W. Vehicle mechanism, a new model for the interpretation of the conductivity of fast proton conductors. *Angew. Chem., Int. Ed.* **1982**, *21*, 208–209.

(30) Ghoufi, A.; Artzner, F.; Malfreyt, P. Physical properties and hydrogen-bonding network of water-ethanol mixtures from molecular dynamics simulations. *J. Phys. Chem. B* **2016**, *120*, 793–802.

(31) Dan, A.; Chakraborty, I.; Ghosh, S.; Moulik, S. P. Interfacial and bulk behavior of sodium dodecyl sulfate in isopropanol water and in isopropanol. *Langmuir* **2007**, *23*, 7531–7538.

(32) Dong, Q.; Yu, C.; Li, L.; Nie, L.; Li, D.; Zang, H. Near-infrared spectroscopic study of molecular interaction in ethanol-water mixtures. *Spectrochim. Acta, Pt. A: Mol. Spectrosc.* **2019**, *222*, 117183.

(33) Jiang, M.; Tan, J.; Chen, Y.; Zhang, W.; Chen, P.; Tang, Y.; Gao, Q. Promoted electrocatalytic hydrogenation of furfural in a biphasic system. *Chem. Commun.* **2023**, *59*, 3103–3106.

(34) Ji, K.; Liu, Y.; Wang, Y.; Kong, K.; Li, J.; Liu, X.; Duan, H. Steering Selectivity in Electrocatalytic Furfural Reduction via Electrode-Electrolyte Interface Modification. *J. Am. Chem. Soc.* **2024**, *146*, 11876–11886.

(35) Zhang, W.; Ge, W.; Qi, Y.; Sheng, X.; Jiang, H.; Li, C. Surfactant Directionally Assembled at the Electrode-Electrolyte Interface for Facilitating Electrocatalytic Aldehyde Hydrogenation. *Angew. Chem., Int. Ed.* **2024**, *63*, No. e202407121.

(36) de Aguiar, H. B.; Strader, M. L.; de Beer, A. G.; Roke, S. Surface structure of sodium dodecyl sulfate surfactant and oil at the oil-in-water droplet liquid/liquid interface: a manifestation of a non-equilibrium surface state. *J. Phys. Chem. B* **2011**, *115*, 2970–2978.

(37) Cui, X.; Mao, S.; Liu, M.; Yuan, H.; Du, Y. Mechanism of surfactant micelle formation. *Langmuir* **2008**, *24*, 10771–10775.

(38) Ahmadi, M.; Aliabadian, E.; Liu, B.; Lei, X.; Khalilpoorkordi, P.; Hou, Q.; Wang, Y.; Chen, Z. Comprehensive review of the interfacial behavior of water/oil/surfactant systems using dissipative particle dynamics simulation. *Adv. Colloid Interface Sci.* **2022**, *309*, 102774.

(39) Hosseinpour, S.; Gotz, V.; Peukert, W. Effect of surfactants on the molecular structure of the buried oil/water interface. *Angew. Chem., Int. Ed.* **2021**, *60*, 25143–25150.

(40) Choi, S.; Parameswaran, S.; Choi, J. H. Understanding alcohol aggregates and the water hydrogen bond network towards miscibility in alcohol solutions: graph theoretical analysis. *Phys. Chem. Chem. Phys.* **2020**, *22*, 17181–17195.

(41) Ghoraiishi, M. S.; Hawk, J. E.; Phani, A.; Khan, M. F.; Thundat, T. Clustering mechanism of ethanol-water mixtures investigated with photothermal microfluidic cantilever deflection spectroscopy. *Sci. Rep.* **2016**, *6*, 23966.

(42) Li, P.; Jiang, Y.; Hu, Y.; Men, Y.; Liu, Y.; Cai, W.; Chen, S. Hydrogen bond network connectivity in the electric double layer dominates the kinetic pH effect in hydrogen electrocatalysis on Pt. *Nat. Catal.* **2022**, *5*, 900–911.

(43) Krishna, R. v. B.; van Baten, J. M. Water/Alcohol Mixture Adsorption in Hydrophobic Materials: Enhanced Water Ingress Caused by Hydrogen Bonding. *ACS Omega* **2020**, *5*, 28393–28402.